Proc. Natl. Acad. Sci. USA
Vol. 95, pp. 15206–15211, December 1998
Biochemistry

Structural invariance of constitutively active and inactive mutants of *Acanthamoeba* myosin IC bound to F-actin in the rigor and ADP-bound states

BRIDGET O. CARRAGHER*†, NAIQIAN CHENG†‡, ZHEN-YUAN WANG†§, EDWARD D. KORN§¶, AMY REILEIN*, DAVID M. BELNAP‡, JOHN A. HAMMER III§, AND ALASDAIR C. STEVEN‡

*Imaging Technology Group, Beckman Institute, University of Illinois, Urbana, IL 61801; and ‡Laboratory of Structural Biology, National Institute of Arthritis, Musculoskeletal and Skin Diseases, and §Laboratory of Cell Biology, National Heart, Lung and Blood Institute, National Institutes of Health, Bethesda, MD 20892

Contributed by Edward D. Korn, October 23, 1998

ABSTRACT **The three single-headed monomeric myosin I isozymes of *Acanthamoeba castellanii* (AMIs)—AMIA, AMIB, and AMIC—are among the best-studied of all myosins. We have used AMIC to study structural correlates of myosin's actin-activated ATPase. This activity is normally controlled by phosphorylation of Ser-329, but AMIC may be switched into constitutively active or inactive states by substituting this residue with Glu or Ala, respectively. To determine whether activation status is reflected in structural differences in the mode of attachment of myosin to actin, these mutant myosins were bound to actin filaments in the absence of nucleotide (rigor state) and visualized at 24-Å resolution by using cryoelectron microscopy and image reconstruction. No such difference was observed. Consequently, we suggest that regulation may be affected not by altering the static (time-averaged) structure of AMIC but by modulating its dynamic properties, i.e., molecular breathing. The tail domain of vertebrate intestinal brush-border myosin I has been observed to swing through 31° on binding of ADP. However, it was predicted on grounds of differing kinetics that any such effects with AMIC should be small [Jontes, J. D., Ostap, E. M., Pollard, T. D. & Milligan, R. A. (1998) *J. Cell Biol.* 141, 155–162]. We have confirmed this hypothesis by observing actin-associated AMIC in its ADP-bound state. Finally, we compared AMIC to brush-border myosin I and AMIB, which were previously studied under similar conditions. In each case, the shape and angle of attachment to F-actin of the catalytic domain is largely conserved, but the domain structure and disposition of the tail is distinctively different for each myosin.**

The myosin superfamily comprises 15 classes of protein distinguished by the sequences of their catalytic domains but also differing in the domain organization of their tails (for reviews, see refs. 1–3). The two largest and best-studied classes are conventional (double-headed, filament-forming) class II myosins and unconventional (single-headed, monomeric) class I myosins. Class I was the first of the 14 classes of unconventional myosins to be discovered. The first known class I myosins, and arguably still the best biochemically described unconventional myosins of any class, are the myosins I of *Acanthamoeba castellanii* (4, 5).

Each of the three AMI isozymes consists of a single, relatively short (for myosins) heavy chain and a single light chain (6). The heavy chain has an ≈72-kDa N-terminal catalytic domain that, as with all myosins, has an ATPase site and an ATP-sensitive actin-binding site. Importantly, a single Ser or Thr residue in their catalytic domains at a position occupied by a Glu or Asp in most other myosins (1) must be phosphorylated for full expression of their actin-activated ATPase activities (6, 7). Distal to the catalytic domain is a single 6-kDa IQ domain (the presumptive light chain-binding site) followed by a ≈50-kDa tail. The tail contains three distinctive regions: a basic, phospholipid-binding region; a Gly-Pro-Ala-rich (GPA) region that contains a second (ATP-insensitive) actin-binding site; and a *src*-homology 3 domain (SH3). The three regions are sequential in AMIB, but the SH3 domain splits the GPA region in AMIC (cf. Fig. 1).

Similar myosins I occur in a wide variety of species, but there are also myosins I that lack the GPA and SH3 regions, and there are others with multiple, sequential, IQ domains (1–3, 8). Intestinal brush-border myosin I (BBMI) is the archetypical example of the latter, with a tail that contains three (9, 10) and, in a minor isoform, four (11) IQ domains and a phospholipid-binding basic region but that has neither a GPA region nor an SH3 domain (Fig. 1). The AMIC light chain has been cloned and sequenced (12) and found not to be calmodulin, unlike the light chains of BBMI.

There have been recent cryoelectron microscopic studies of the actin complexes of chicken intestinal BBMI (13–15) and of unphosphorylated (but not of phosphorylated) AMIB (16). The angle at which the catalytic domain attaches to F-actin was reported (16) to be ≈10% more acute for AMIB than for BBMI, and the tail of AMIB was shown to be more compact than the tail of BBMI. It was speculated that the angle of attachment of phosphorylated AMIB may be more similar to that of BBMI. Also, binding of Mg-ADP was found to cause a 31° swing of the BBMI tail (13, 15) and to have a similar effect on subfragment 1 of smooth muscle myosin II (17) but no effect on skeletal muscle myosin II. For these myosins, the ADP-induced transition correlates with differences in the kinetics of the respective actin-activated ATPases (18). Specifically, the release of ADP from the actomyosin complex is significantly slower for BBMI (18) and for smooth muscle myosin II (18) than for skeletal muscle myosin II. Because the kinetics of AMIA and AMIB resemble those of skeletal muscle myosin II (19), it was predicted that ADP binding to the AMI myosins should cause little structural change (18).

In the accompanying paper (6), it is shown that the mutant S329E is constitutively active, indistinguishably so from phosphorylated wild-type AMIC, whereas S329A is constitutively inactive, like unphosphorylated wild-type AMIC. Thus, the structures of the actin complexes of S329A and S329E should reproduce those of unphosphorylated and phosphorylated

The publication costs of this article were defrayed in part by page charge payment. This article must therefore be hereby marked "*advertisement*" in accordance with 18 U.S.C. §1734 solely to indicate this fact.

Abbreviations: AMIC, *Acanthamoeba* myosin IC; BBMI, brush border myosin I.

†B.O.C., N.C., and Z.-Y.W. contributed equally to this project.

¶To whom reprint requests should be addressed at: Building 3, Room B1-22, MSC 0301, National Institutes of Health, Bethesda, MD 20892-0301. e-mail: edk@nih.gov.

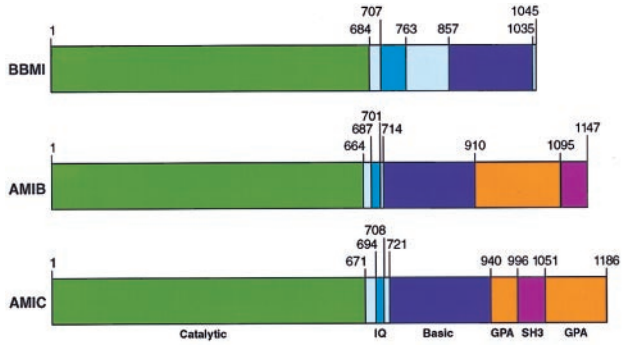

FIG. 1. Domain maps of vertebrate intestinal BBMI and two isoforms of *Acanthamoeba castellanii* myosin I, AMIB and AMIC.

wild-type AMIC, respectively. Therefore, if—as has been suggested (16)—the angle of attachment of wild-type AMIC to F-actin is affected by phosphorylation, the actin complexes of S329E and S329A should differ in this respect. Moreover, Mg-ADP should have little effect on the conformation of S329E bound to F-actin if the magnitude of the structural change in myosins between the Mg-ADP and rigor states does indeed correlate with their ATPase kinetics and assuming that the kinetics of AMIC are similar to those of AMIA and AMIB (19). In this paper, we compare the structures of the actin complexes of S329E and S329A in rigor state and the structure of actin-S329E in the presence of excess Mg-ADP to each other and to the previously determined structures of BBMI and AMIB.

MATERIALS AND METHODS

Proteins. F-actin was prepared as in the accompanying paper (6) and stored for up to 3 weeks on ice in 5 mM Tris (pH 8.0) containing 1 mM DTT and 2 mM $MgCl_2$. The recombinant mutant myosins were expressed in 1- to 3-liter cultures of baculovirus-transfected Sf9 cells by Cell Trends (Middletown, MD), and the cells were harvested, frozen in liquid nitrogen, and stored at −70°C for up to several months. Epitope-tagged myosins were purified by affinity chromatography as described (6) except that, after adsorption of the myosin on the affinity column, the column was washed with 8 vol of buffer A (20 mM imidazole (pH 7.0) containing 50 mM NaCl/1 mM DTT/2 mM $MgCl_2$/0.1 mM EGTA) to remove nucleic acid (as detected by using A_{260}) and phosphate before the myosin was eluted with buffer A containing Flag-peptide (0.3 mg/ml). Fractions (0.6 ml) were collected, analyzed for protein concentration by using the Bradford assay and for purity by using SDS/PAGE, and pooled accordingly. The pooled fractions were concentrated to 3–5 mg/ml, without apparent precipitation, by using a Microcon 30 microconcentrator (Micron Separations, Westboro, MA) at 4°C, stored on ice, and used within 1 week.

Cryoelectron Microscopy. To prepare the rigor complexes, F-actin was diluted to 0.03–0.1 mg/ml in buffer A and, after the filament preparation was checked with negative staining, a 4-μl drop was applied to a perforated carbon grid for ≈1 min. Excess fluid was blotted with filter paper, and a 4-μl drop of AMIC-S329E or AMIC-S329A at 0.3–0.5 mg/ml in buffer A was applied to the grid and incubated for 2 min. The grid was then blotted with filter paper and frozen by quenching in liquid ethane cooled to liquid-nitrogen temperature as described (20). Grid preparation was performed both at room temperature and in a cold room at ≈4°C. To visualize the ADP-bound state, the same procedures were used except that the myosin (S329E) concentration was increased to ≈3.5 mg/ml in buffer A containing 2 mM MgADP and 100 μM diadenosylpentaphosphate (to inhibit myokinase activity present in all actin preparations). The entire process was carried out at 4°C. Frozen grids were transferred into a Gatan 626 cryoholder (Gatan, Warrendale, PA) and observed at 120 keV (1 eV = 1.602×10^{-19} J) in a Philips CM120 electron microscope as described (20). Micrographs were recorded at defocus values of 1.4–2.0 μm at a magnification of about ×45,000 by using minimal electron dose procedures.

Image Analysis and Helical Reconstruction. Micrographs were screened by eye for contrast and appropriate density of filaments and by optical diffraction for image quality and defocus. All micrographs selected for analysis had first zeros of the contrast-transfer function between $(22\ \text{Å})^{-1}$ and $(25\ \text{Å})^{-1}$ They were scanned on a Leaf Scanner (Scitex, Herzlia, Israel) at a rate corresponding to ≈7 Å per pixel at the specimen. Image processing was performed by using the PHOELIX software package essentially as described (21, 22). After computationally straightening the filaments and calculating their Fourier transforms, layer-line data were extracted out to the 14th order (n) on the 58th layer-line ($l = 58$, using the selection rule, $l = 25n + 54m$, where m is any integer), corresponding to a Fourier limit of ≈24 Å. Layer-line data from each transform were adjusted to a common phase origin and then averaged by using one of the filaments as template in an initial round of alignment and averaging. This process was iterated three times using the average from the previous cycle as the template in the next cycle. This average transform was then used as starting point for two rounds of layer-line altitude refinement by the procedure of Morgan and DeRosier (23). Finally, the layer lines were truncated at $24\ \text{Å}^{-1}$ and used to compute a three-dimensional density map. Surface renderings were created by using VOXV1 (http://www.cs.sunysb.edu/~vislab/projects/volvis).

Molecular Modeling. Density maps of segments of filament containing ≈14 molecules each of actin and myosin with voxels of $(5\ \text{Å})^3$ were transferred into the modeling program O (24) and displayed as wire-mesh figures. The molecular model, a truncated version of the myosin II structure of Rayment *et al.* (25), was docked manually as a rigid body into the cryoelectron microscopy-derived envelope as contoured to enclose 100% of expected mass. The map and model were then rotated and their fit refined from a different viewing angle. This process was iterated until no further improvement was obtained.

RESULTS

Visualization of AMIC Binding to F-Actin. Cryomicrographs of actin filaments quantitatively decorated with AMIC molecules are shown in Fig. 2. These images compare the rigor state of the constitutively active mutant (S329E), the rigor state of the constitutively inactive mutant (S329A), and the ADP state of S329E. At first sight, the filaments with ADP-bound myosin have a somewhat different appearance, but this impression simply reflects that the images are noisier as a result of their heavy background of unbound myosin molecules (see below). This background was incurred because binding of ADP by AMIC substantially reduces its affinity for actin filaments, so that it proved necessary to increase the myosin concentration 10-fold to achieve saturating levels of decoration.

Helical reconstructions were calculated for all three kinds of filaments. The details of the reconstructions are summarized in Table 1. The microscopy conditions and the cumulative lengths of filaments analyzed were similar in each case, and all three density maps have a resolution of ≈24 Å. Because the quality of all three maps is uniform, differences in visualized structure should reflect properties of the filament proteins, not technical differences between the respective analyses. However, the predominant impression from comparing the three density maps is that they are indeed very similar, i.e., the structure of the AMIC molecule

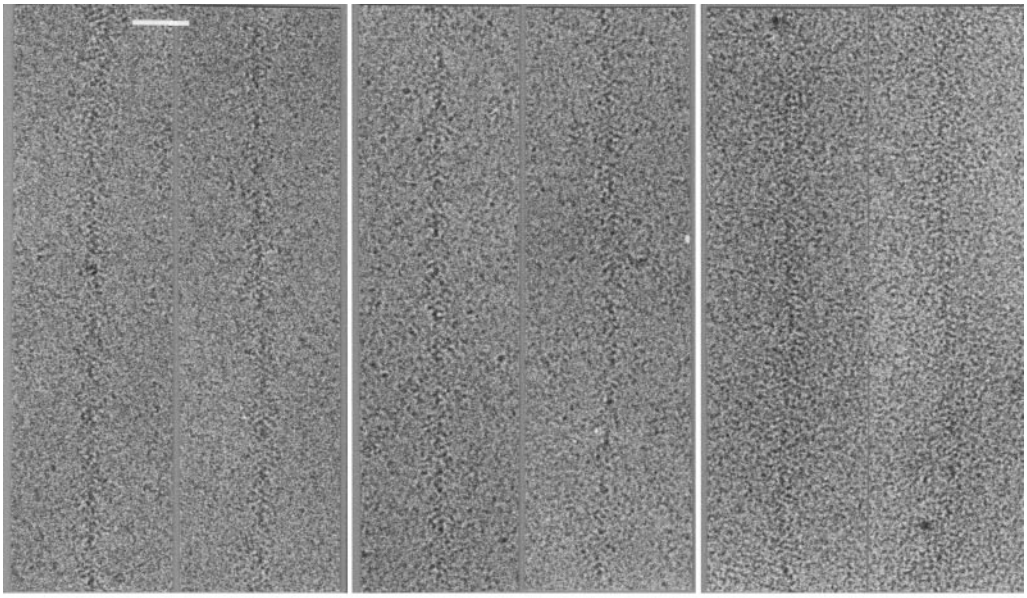

FIG. 2. Cryoelectron micrographs of actin filaments decorated with variants of *Acanthamoeba* myosin, AMIC. (*a*) constitutively active mutant, S329E, rigor state; (*b*) constitutively inactive mutant, S329A, rigor state; (*c*) constitutively active mutant, S329E, ADP-bound state. (Bar = 500 Å.)

and its mode of attachment to the actin filament is much the same in all three cases. The reconstructions show elongated AMIC molecules extending in a distinctive conformation from the actin filament (Fig. 3 *a–c*). The ovoid domain in immediate contact with the actin filament is essentially identical in shape in all three maps. This domain extends into the tail region (Fig. 3 *a–c*), which consists of a curved tubular segment 25–30 Å in diameter terminating in a distal knob. The overall length of AMIC is ≈145 Å.

Molecular Modeling of Actin-Bound AMIC. To interpret these molecular volumes in greater detail, we performed modeling based on the crystal structure of chicken skeletal myosin II (25). Assuming that regions of high sequence homology correspond to conserved three-dimensional structure, we obtained a model for the AMIC catalytic domain by referring to a sequence alignment of the two molecules (1). Thus, the coordinates of residues 80–783 of the myosin II sequence were used for residues 1–669 of the AMIC heavy chain. We docked this model into our S329E-rigor map (Fig. 4*a*) by using the graphics program O (24) to obtain a best fit under visual criteria (see *Materials & Methods*).

For the portion of AMIC closest to the actin filament, the fit obtained was excellent. The molecular model closely follows the contours of the EM-derived envelope (Fig. 4*a*), whose asymmetries are such as to make the fit unique. Only a few loops protrude slightly from the envelope. The two loops marked in Fig. 4*a* (white arrows) correspond to peptides of locally divergent sequence that would not be expected to be structurally conserved. The overall fidelity of the fit confirms the reliability of the model and implies that the rest of the envelope is occupied by the remaining portions of AMIC (residues 670–1,186 plus the 16.7-kDa light chain, corresponding to ≈45% of the total mass). In the distal portion of the ovoid domain, the model does not fully occupy the space enclosed by the molecular envelope (blue arrow in Fig. 4*a*), and we infer that the unoccupied portion contains parts of AMIC not accounted for in our model. Because the adjacent portion of heavy-chain sequence is the IQ region (which is thought to bind the light chain) it may be that these moieties reside in this part of the envelope. Crystal structures have been determined for SH3 domains (e.g., ref. 28), but because this component is small (≈55 residues) and we have no firm evidence as to its location in the AMIC tail, this component has not been modeled.

Table 1. Parameters of three-dimensional reconstructions of myosin configurations

Myosin (state)	No. of reconstructions (micrographs)	No. of actomyosin molecules	Mean phase residual (degrees)
S329E (rigor)	26 (5)	4,752	28 (20–40)
S329A (rigor)	22 (4)	3,402	30 (20–44)
S329E (Mg-ADP)	25 (6)	4,536	36 (21–43)

Each density map combined the stated number of individual reconstructions (usually two reconstructions per filament, corresponding to the near and far sides) from the stated number of micrographs, which together contained the stated number of actomyosin molecules. The internal consistency of each data set is expressed in terms of the mean phase residual over all strong layer lines out to an axial spacing of 24 $Å^{-1}$, averaged over the full data set. The numbers in parentheses give the range of this residual for individual filaments in the data set.

Because the molecular envelopes of the rigor complexes of acto-S329E and acto-S329A are essentially superimposable (Fig. 4*b*), one would expect the placement of the AMIC catalytic domain in the acto-S329E rigor map to apply equally well to the acto-S329A rigor map, which proved to be the case (data not shown).

The same results held true when the AMIC catalytic domain model was inserted into the map of S329E-ADP (Fig. 4*c*). In this case, the molecular envelopes coincide closely over the catalytic domain but do not rule out a small rotation of the distal part of the tail between the ADP and rigor states (see Fig. 4*c*). Such a rotation would be of the order of ≈2.5°, equivalent to a translation of ≈5 Å at the distal tip. However, any such movement is so small as to be marginally significant at our current resolution, and it is clear that any such transition is miniscule compared with the large movements observed for BBMI (15) and smooth muscle myosin (17).

We also used modeling to compare AMIC's mode of binding to F-actin with that of AMIB. The same myosin model was docked into the density map of Jontes *et al.* (16) for unphosphorylated acto-AMIB, and the results were compared. The fits were essentially identical. The vector along the long axis of the catalytic domain (between residues

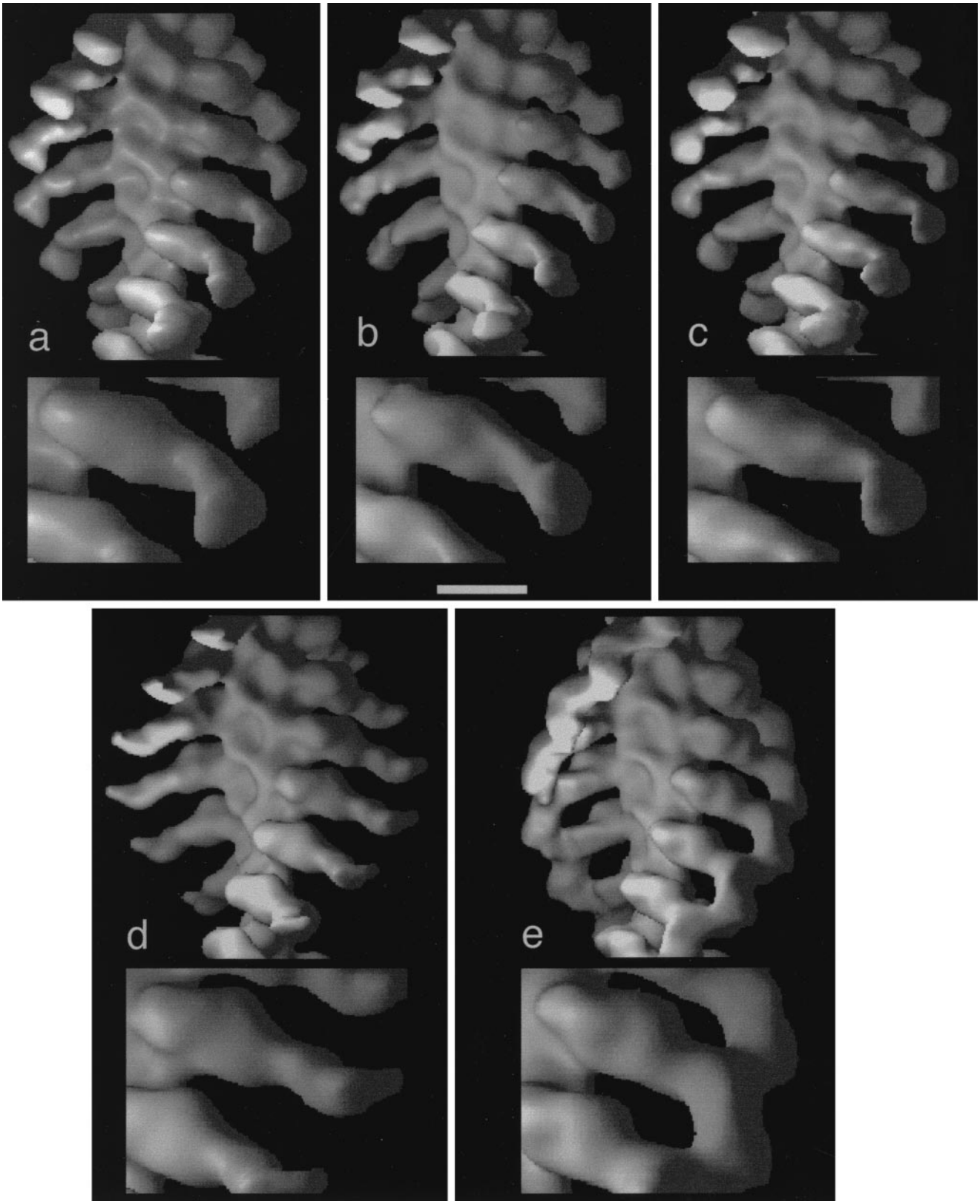

FIG. 3. Surface rendering of the three-dimensional reconstructions of actin filaments decorated with myosin AMIC. (*a*) constitutively active mutant, S329E, rigor state; (*b*) constitutively inactive mutant, S329A, rigor state; (*c*) constitutively active mutant, S329E, ADP-bound state. Also shown to allow direct comparison with other myosins I are BBMI reproduced from ref. 15 (*d*) and AMIB reproduced from ref. 17 (*e*). In each case, a filament segment containing approximately 14 molecules is shown along with a blow-up showing side views of the attached myosin I molecules. (Bar = 50 Å for blowups.)

389 and 689 of the myosin II sequence) differs in orientation by less than 0.5° between the two fits. Because the actin-binding geometry for AMIC is indistinguishable between the active (S329E) and inactive (S329A) forms, we suggest that active, i.e., phosphorylated, AMIB also binds at the same angle (cf. ref. 16).

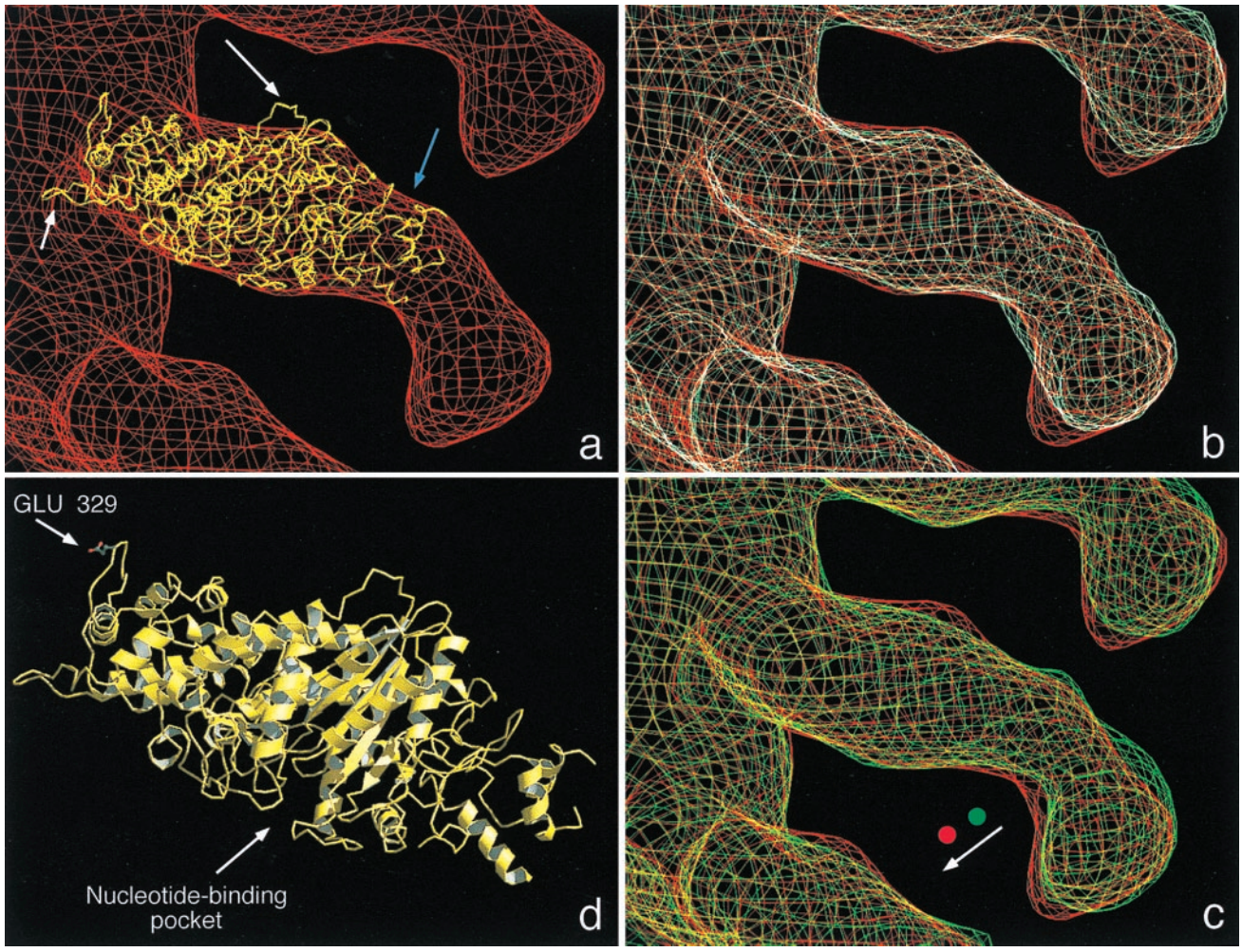

FIG. 4. (*a*) A molecular model of the catalytic domain of AMIC (yellow) was docked into the cryoelectron microscopy density map of the F-actin-AMIC (S329E) complex in rigor state (red). The model used for AMIC is the crystal structure of residues 80–783 of chicken smooth muscle myosin II (25). In the actin-proximal portion of the AMIC envelope, the model fits snugly, but toward the distal part of this domain (blue arrow), the volume is not fully occupied. The white arrows indicate two loops that protrude through the envelope, corresponding to sequences that are not conserved between the two myosins. Long arrow = D450 to Q456 of myosin II; short arrow = F366 to G379 of myosin II. (*b*) Superimposition of the molecular envelopes of the constitutively active mutant, S329E (red) and the constitutively inactive mutant, S329A (cyan), in rigor. (*c*) Superimposition of the constitutively active mutant, S329E, in its rigor (red) and ADP-bound (green) states. The shapes of the distal portion of the tail are essentially the same and suggest a small rigid-body rotation (see arrow) between the two states, about an axis near the midpoint of the myosin molecule. (*d*) Ribbon diagram of the model of the AMIC catalytic domain based on the crystal structure of chicken skeletal muscle myosin II (25). The positions of the regulatory residue at position 329 in the AMIC sequence (corresponding to position 411 in the muscle myosin) and of the nucleotide-binding pocket are marked. The model is in the same orientation from which AMIC is viewed in *a*–*c*. The diagram was prepared by using RASTER3D (26) and MOLSCRIPT (27).

DISCUSSION

Two questions were addressed in this study. (*i*) Do structural differences exist between the constitutively active and inactive variants of AMIC in their rigor conformations that may offer clues as to how regulation is effected? (*ii*) Do structural changes take place in AMIC on switching between the rigor and ADP states? In both cases, we found any such differences to be negligible at our current resolution (24 Å). To facilitate discussion of these observations, the model used for the AMIC motor domain is shown in Fig. 4*d*, as viewed from the same direction as in our cryoelectron microscopy maps (Figs. 4 *a*–*c*).

Regulation. All observations to date indicate that the catalytic domains of myosins have closely conserved structures. Also invariant is their mode of binding to actin, which is essentially the same for all myosins and functional states imaged thus far. However, it is clear that events at well separated sites on the catalytic domain can affect each other. Thus, a negative charge on the key regulatory residue (position 329 in AMIC) is essential for actin-mediated ATPase activity in the nucleotide binding pocket ≈60 Å away (ref. 25; cf. Fig. 4*d*). Conversely, binding of ADP at the latter site reduces (and binding of ATP further reduces) myosin's binding affinity for actin, presumably by inducing structural changes at sites that interact with the actin filament.

Glu-411, the myosin II residue that corresponds to Ser-329 of AMIC, resides at the tip of the so-called HCM loop (ref. 1; Fig. 4*d*), and it is plausible that a similar loop exists on AMIC. This loop is thought to make contact with the actin filament (29), although this has been questioned (30). Because the overall static (i.e., time-averaged) structure of the catalytic domain is indistinguishable between the active (S329E) and inactive (S329A) forms (cf. Figs. 3 *a* and *b* and 4 *b* and *c*), it may be that dynamic aspects of the molecule—for instance, "breathing" motions (31) or the on/off rate for actin binding—are important for ATPase activity and are affected by the interaction of this loop with actin. Breathing also has been invoked to explain the binding of antibodies to internal poliovirus epitopes (32) and the effects of drug binding to rhinovirus (33). In the latter study, altered susceptibility to

proteolysis was used as an index of breathing motion. Consistent with this and with our proposal that breathing may be involved in myosin regulation, an earlier study found that the susceptibility to trypsin of actin-bound AMIA was altered by phosphorylation (34). Concerning the possibility that its on/off rate for actin binding may be involved in regulating the myosin ATPase, an earlier study showed that phosphorylation of AMIA increases its affinity for F-actin in the absence of ATP (35). On the other hand, an alternative explanation of our results is that structural changes in the AMIC catalytic domain do, in fact, accompany regulation, but are too subtle to be seen at our current resolution.

To Swing or Not to Swing? The prediction made on the basis of comparative reaction kinetics (16) that AMIC would emulate skeletal muscle myosin in failing to register a large swing of its tail on switching from the ADP state into rigor is borne out by our observations. However, an explanation for this correlation between kinetics and conformational change is not yet evident. The swings of the tails of BBMI and smooth muscle myosin have been proposed to represent steps in their respective power strokes, and it has been further argued (15) that the full power stroke involves (at least) two distinct steps. In this context, it may be that the relative size of these steps varies from system to system and that, for AMIC, the movement associated with the second step (ADP $\rightarrow$ rigor) happens to be very small. An alternative possibility is that the total translational shift per power stroke varies substantially among different myosins, with BBMI and smooth muscle myosin II representing one extreme (large shifts) and AMIC representing the other extreme. If the efficiency of the biomechanical cycle is approximately uniform (i.e., the same amount of work is realized per ATP hydrolyzed), it may be that—because work = force $\times$ shift—myosins with small shifts exert relatively powerful forces. In this idiom, AMIC would be expected to be a powerful isoform. This proposition is testable by single-molecule mechanical methods.

Myosin Tails. In marked contrast to the conserved shape and disposition of the catalytic domain (head), the tails of all myosins I visualized to date (BBMI, AMIB and AMIC) vary widely in structure (cf. Fig. 3). Although the AMIB tail is similar in molecular weight and domain composition (albeit with some reshuffling) to the AMIC tail (cf. Fig. 1) it extends out of the head domain in a quite different direction, turning axially downwards instead of radially outwards. Moreover, there is clearly no interaction between adjacent AMIC tails (cf. ref. 16). The BBMI tail (Fig. 3*d*) is longer, thinner, and more segmented than the tails of AMIC (Figs. 3*a*) or AMIB (Fig. 3*e*). It seems plausible that, as suggested (15), variations in myosin tails reflect adaptations to various intracellular situations with specialized requirements for vectorial force generation. Presumably, the myosins differ with respect to the receptors to which they bind, the mechanics of their power strokes, and their cooperativity, among other parameters. Understanding these properties in terms of the domain design of their tails is an attractive goal that should be aided by structural studies on an expanded range of myosin molecules.

We appreciate advice and help received from M. Whittaker and Dr. R. Milligan during this project, and their provision of published density maps of acto-BBMI and acto-AMIB. We also thank Dr. B. Bowers for initial negative staining electron microscopy and Dr. C. Hyde for making available a graphics workstation.

1. Sellers, J. R. (1998) in *Protein Profiles*, ed. Sheterline, P. (Academic, London).
2. Mooseker, M. S. & Cheney, R. E. (1995) *Annu. Rev. Cell Dev. Biol.* **11,** 633–675.
3. Hammer, J. A., III (1994) *J. Muscle Res. Cell Motil.* **15,** 1–10.
4. Pollard, T. D. & Korn, E. D. (1973) *J. Biol. Chem.* **248,** 4682–4690.
5. Pollard, T. D. & Korn, E. D. (1973) *J. Biol. Chem.* **248,** 4691–4697.
6. Wang, Z.-Y., Wang, F., Sellers, J. R., Korn, E. D. & Hammer, J. A., III (1998) *Proc. Natl. Acad. Sci. USA* **95,** 15200–15205.
7. Brzeska, H., Lynch, T. J., Martin, B. M. & Korn, E. D. (1989) *J. Biol. Chem.* **264,** 19340–19348.
8. Ruppert, C., Kroschewski, R. & Bahler, M. (1993) *J. Cell Biol.* **120,** 1393–1403.
9. Hoshimaru, M. & Nakanishi, S. (1987) *J. Biol. Chem.* **262,** 14625–14632.
10. Garcia, A., Coudrier, E., Carboni, J., Anderson, J., Vandekerckhove, J., Mooseker, M., Louvard, D. & Arpin, M. (1989) *J. Cell Biol.* **109,** 2895–2903.
11. Halsall, D. J. & Hammer, J. A., III (1990) *FEBS Lett.* **267,** 126–130.
12. Wang, Z.-Y., Sakai, J., Matsudaira, P. T., Baines, I. C., Sellers, J. R., Hammer, J., III, & Korn, E. D. (1997) *J. Muscle Res. Cell Motil.* **18,** 395–398.
13. Jontes, J. D., Wilson-Kubalek, E. M. & Milligan, R. A. (1995) *Nature (London)* **378,** 751–753.
14. Jontes, J. D. & Milligan, R. A. (1997) *J. Mol. Biol.* **266,** 331–342.
15. Jontes, J. D. & Milligan, R. A. (1997) *J. Cell Biol.* **139,** 683–693.
16. Jontes, J. D., Ostap, E. M., Pollard, T. D. & Milligan, R. A. (1998) *J. Cell Biol.* **141,** 155–162.
17. Whittaker, M., Wilson-Kubalek, E. M., Smith, J. E., Faust, L., Milligan, R. A. & Sweeney, H. L. (1995) *Nature (London)* **378,** 748–751.
18. Jontes, J. D., Milligan, R. A., Pollard, T. D. & Ostap, E. M. (1997) *Proc. Natl. Acad. Sci. USA* **94,** 14332–14337.
19. Ostap, E. M. & Pollard, T. D. (1996) *J. Cell Biol.* **132,** 1053–1060.
20. Conway, J. F., Duda, R. L., Cheng, N., Hendrix, R. W. & Steven, A. C. (1995) *J. Mol. Biol.* **253,** 86–99.
21. Carragher, B., Whittaker, M. & Milligan, R. (1996) *J. Struct. Biol.* **116,** 107–112.
22. Whittaker, M., Carragher, B. O. & Milligan, R. (1995) *Ultramicroscopy* **58,** 245–259.
23. Morgan, D. G. & DeRosier, D. J. (1995) *Ultramicroscopy* **46,** 263–285.
24. Jones, T. A., Zou, J. Y., Cowan, S. W. & Kjeldgaard, M. (1991) *Acta Crystallogr. A* **47,** 110–119.
25. Rayment, I., Rypniewski, W. R., Schmidt-Base, K., Smith, R., Tomchick, D. R., Benning, M. M., Winkelmann, D. A., Wesenberg, G. & Holden, H. M. (1993) *Science* **261,** 50–58.
26. Merritt, E. A. & Bacon, D. J. (1997) *Methods Enzymol.* **277,** 505–524.
27. Kraulis, P. J. (1991) *J. Appl. Crystallogr.* **24,** 946–950.
28. Feng, S., Chen, J. K., Yu, H., Simon, A. & Schreiber, S. L. (1994) *Science* **266,** 1241–1247.
29. Rayment, I., Holden, H. M., Whittaker, M., Yohn, C. B., Lorenz, M., Holmes, K. C. & Milligan, R. A. (1993) *Science* **261,** 58–65.
30. Mendelson, R. & Morris, E. P. (1997) *Proc. Natl. Acad. Sci. USA* **94,** 8533–8538.
31. Englander, W. & Mayne, A. (1993) *Annu. Rev. Biophys. Biomol. Struct.* **21,** 243–265.
32. Li, Q., Yafal, A. G., Lee, Y. M. H., Hogle, J. & Chow, M. (1994) *J. Virol.* **68,** 3965–3970.
33. Lewis, J, K, Bothner, B., Smith, T. J. & Siuzdak, G. (1998) *Proc. Natl. Acad. Sci. USA* **95,** 6774–6778.
34. Brzeska, H., Lynch, T. J. & Korn, E. D. (1989) *J. Biol. Chem.* **264,** 10243–10250.
35. Lynch, T. J., Albanesi, J. P., Korn, E. D., Robinson, E. A., Bowers, B. & Fujisaki, H. (1986) *J. Biol. Chem.* **261,** 17156–17162.